Published in ""Proceedings of the National Academy of Sciences
109(17): 6457-6462 , 2012"
which should be cited to refer to this work.

http://doc.rero.ch

Dynamical quantum Hall effect in the parameter space

V. Gritsev[a] and A. Polkovnikov[b,1]

[a]Physics Department, University of Fribourg, Chemin du Musee 3, 1700 Fribourg, Switzerland and [b]Physics Department, Boston University, Commonwealth Avenue 590, Boston MA, 02215

Geometric phases in quantum mechanics play an extraordinary role in broadening our understanding of fundamental significance of geometry in nature. One of the best known examples is the Berry phase [M.V. Berry (1984), Proc. Royal. Soc. London A, 392:45], which naturally emerges in quantum adiabatic evolution. So far the applicability and measurements of the Berry phase were mostly limited to systems of weakly interacting quasi-particles, where interference experiments are feasible. Here we show how one can go beyond this limitation and observe the Berry curvature, and hence the Berry phase, in generic systems as a nonadiabatic response of physical observables to the rate of change of an external parameter. These results can be interpreted as a dynamical quantum Hall effect in a parameter space. The conventional quantum Hall effect is a particular example of the general relation if one views the electric field as a rate of change of the vector potential. We illustrate our findings by analyzing the response of interacting spin chains to a rotating magnetic field. We observe the quantization of this response, which we term the rotational quantum Hall effect.

Berry curvature | geometric tensor | quantum dynamics | quantum geometry | quantum Hall effect

In quantum mechanics the Berry phase is defined as a phase accumulated by the wave function during the adiabatic evolution around a closed path in the parameter space denoted by $\vec{s}$. This phase can be obtained by integrating the Berry connection:

$$\mathscr{A}_\mu = i\langle\psi|\partial_\mu|\psi\rangle \qquad [1]$$

along this path (1). Here to shorten notations we define $\partial_\mu \equiv \partial_{s_\mu}$. The vector $\vec{s}$ stands for an arbitrary set of parameters which change during the adiabatic evolution. These can be a coordinate of a particle, its momentum, magnetic or electric field, vector potential, pressure, volume, a coupling to some external potential, and so force. From the definition above it is clear that the Berry phase has a purely geometric interpretation. Together with the Berry connection $\mathscr{A}_\mu$ (analogous to the vector potential in the parameter space), one defines the Berry curvature (analogous to the magnetic field):

$$\mathscr{F}_{\mu\lambda} = \partial_\mu \mathscr{A}_\lambda - \partial_\lambda \mathscr{A}_\mu. \qquad [2]$$

From the Stokes theorem it follows that the Berry phase along some closed path can be found by integrating the Berry curvature over the area enclosed by this path. A nontrivial Berry phase—i.e., the phase not equal to 0 or π—and a nonzero Berry curvature are in general associated with a broken time-reversal symmetry, because otherwise all wave functions can be made real (2).

The Berry curvature is directly related to the geometric tensor (3) introduced to describe manifolds of adiabatically connected wave functions $\psi(\vec{s})$:

$$\chi_{\mu\lambda} = \langle\psi|\overleftarrow{\partial}_\mu\partial_\lambda|\psi\rangle - \langle\psi|\overleftarrow{\partial}_\mu|\psi\rangle\langle\psi|\partial_\lambda|\psi\rangle \qquad [3]$$

It is straightforward to check that $\mathscr{F}_{\mu\lambda} = -2\Im[\chi_{\mu\lambda}]$, while $g_{\mu\lambda} = \Re[\chi_{\mu\lambda}]$ defines the Riemannian metric tensor associated with the same manifold. The Riemann curvature associated with the above metrics as well as the components of the geometric tensor can serve as observable independent measures of singularities like phase transitions (4). The geometric tensor can be extended to mixed states by taking the statistical average of the geometric tensor associated with individual pure states .

The Berry phase and related concepts found multiple applications in many different quantum and classical systems. In particular, it underlies the Aharonov-Bohm effect; it shows up in transport in graphene in a quantum Hall regime (5); it can emerge in photon interference of a circularly polarized light (6, 7); it appears in anomalous quantum Hall effect in magnetic metals (8), in various magnetoelectric response functions (9), in Thouless pumps (10, 11) and many other phenomena, including various forms of solid-state related topological phenomena like topological insulators [see Ref. (12) for a recent review]. Most known applications of the Berry phase and ways to experimentally measure it rely on existence of free or nearly free quasi-particles which can independently interfere affecting transport properties. If the concept of quasi-particles is ill defined and transport experiments are not feasible, like in cold atom systems, the Berry phase could not be measured using traditional approaches.

Results

The main finding of our paper is that in slowly driven isolated systems the Berry curvature emerges in a linear response of physical observables to the quench velocity $\vec{v} = \dot{\vec{s}}$. Specifically we show that if the quench velocity $\vec{v}$ is aligned along the λ direction in the parameter space then measuring the response of the generalized force along the μ-direction: $\mathscr{M}_\mu = -\langle\psi(t_f)|\partial_\mu\mathscr{H}|\psi(t_f)\rangle$ gives the $\lambda\mu$ component of the Berry curvature:

$$\mathscr{M}_\mu = \text{const} + \mathscr{F}_{\mu\lambda}v_\lambda + \mathscr{O}(v^2). \qquad [4]$$

where we used the Einstein convention of summation over repeated indexes. The constant term gives the value of the generalized force in the adiabatic limit. This result is very remarkable since it shows that even without dissipation, the leading nonadiabatic response of a quantum system is local in time. Indeed it is determined by the instantaneous velocity and the instantaneous matrix elements and the instantaneous spectrum. We sketch the details of the derivation of Eq. **4** in the *Methods* section. Here we only point that this result is valid if either of the three conditions are met: (*i*) the velocity $\vec{v}$ is turned on smoothly, (*ii*) the system is prepared initially in a state with a large gap, (*iii*) there is a weak dephasing mechanism in the system and the time of experiment is longer than the dephasing time. The first two conditions imply that the system is not excited at the initial time of the evolution, and the last condition implies that even if there are small excitations in the system, they come with a random phase. Note that the

Author contributions: A.P. and V.G. designed and performed research; and V.G. and A.P. wrote the paper.

The authors declare no conflict of interest.

This article is a PNAS Direct Submission.

[1]To whom correspondence should be addressed. E-mail: asp@bu.edu.

dephasing does not have to be due to external noise, it can be due to averaging of over different experimental runs with slightly fluctuating durations. The Eq. **4** applies to both gapless and gapped systems at either zero or at finite temperatures. It can be used for a single particle and for an interacting many-body system in a thermodynamic limit. However, we need to keep in mind that the Berry curvature is a susceptibility, in particular it can be expressed through the nonequal time correlation functions: (1)

$$\mathcal{F}_{\mu\lambda} = -i \int_0^\infty dt\, t \langle [\partial_\mu \mathcal{H}(t), \partial_\lambda \mathcal{H}(0)] \rangle_0. \qquad \textbf{[5]}$$

Here $\partial_\mu \mathcal{H}(t)$ stands for the operator $\partial_\mu \mathcal{H}$ in the Heisenberg representation with respect to the instantaneous Hamiltonian, $[\ldots]$ stands for the commutator, and the subindex 0 means that the average is taken with respect to the adiabatically evolved state (e.g., the instantaneous ground state if the system is initially prepared at zero temperature). As usual, we assume that the energies have infinitesimal positive imaginary parts to guarantee the convergence of the integral above. In low dimensional gapless systems or near phase transitions, the Berry curvature can diverge. Then the linear response theory breaks down and the dependence $\mathcal{M}_\mu(v_\lambda)$ can become nonanalytic. In this work we will not be concerned with these quite special situations. Let us point out that in large systems if we are dealing with extensive couplings, the Berry curvature is also extensive. Therefore possible nonextensive number of degeneracies of the ground state does not affect the result Eq. **4**. However, these degeneracies can affect topological protection of the integer Chern numbers associated with the Berry curvature which we discuss below. Let us also point out that Eq. **4** implies that the nonvanishing linear response coefficient indicates a broken time-reversal symmetry in the Hamiltonian (possibly by the coupling s_μ). This situation is opposite to that in the imaginary time dynamics, where the linear response for a similar protocol reveals the symmetric part of the geometric tensor (13). The latter is nonsensitive to the time-reversal symmetry.

The Eq. **4** can be interpreted as a Hall effect in the abstract parameter space. Indeed then v_λ can be interpreted as a driving current in λ-direction. The response $\mathcal{M}_\mu$ is analogous to the electric field in the transverse direction and then $\mathcal{F}_{\lambda\mu}$ is the analogue of the Hall resistance. Conversely by s_λ we can understand the electric field component in the x-direction (which can be viewed as a rate of change of the x-component of the vector potential). Similarly by s_μ we can understand the vector potential along y-direction. Then the corresponding generalized force $\mathcal{M}_\mu = -\partial_\mu \mathcal{H}$ is proportional to the y-component of the current. Then up to the coupling e^2/h the Berry curvature is given by the Hall conductivity and Eq. **4** reduces to the well-known result (see *Methods* for more details). Different variations of Eq. **4** also appeared earlier in other particular contexts (11, 14).

The proposed method of finding the Berry curvature has another significant advantage over traditional interference based methods. Namely, it does not require strict adiabaticity, which is nearly impossible to achieve in large interacting systems. Contrary, the applicability of the linear response regime, where Eq. **4** is valid, only requires that intensive quantities like the magnetization per unit volume remain small. Therefore, there are no difficulties related to taking the thermodynamic limit with possible exceptions near singularities like critical points where the Berry curvature can diverge. The relation (**4**) gives a clear route for measuring the Berry curvature and consequently the Berry connection and the Berry phase in generic systems. A possible procedure can consist of evolving the system initially prepared in the ground state by quenching some tuning parameter s_λ smoothly in time. Then at the time $t = 0$ corresponding to the Hamiltonian of interest, one measures the generalized force corresponding to a different parameter s_μ : $\mathcal{M}_\mu$. Repeating these measurements at different velocities one can extract the slope of $\mathcal{M}_\mu(v_\lambda)$, which coincides with the Berry curvature. One can repeat the same sequence at different values of $\vec{s}$ confined within some closed area of the parameter space and evaluate the Berry phase using the Stokes theorem. The relation (**4**) also extends to weak continuous measurements. Then the Berry curvature can be extracted from the linear in velocity correction to $\mathcal{M}_\mu$.

If the parameter field $\vec{s}$ lies on an arbitrary compact manifold (surface) $\mathcal{S}$ like a sphere or a torus, then the integral over the Berry curvature for a given state $|\psi\rangle$ forms a topological integer invariant known as the first Chern number:

$$ch_1(|\psi\rangle) = \frac{1}{2\pi} \int_{\mathcal{S}} dS_{\mu\lambda} \mathcal{F}_{\mu\lambda}. \qquad \textbf{[6]}$$

where $dS_{\mu\lambda}$ is an area form element in the parameter space. To observe the quantization it is important that the gap separating the ground state from the rest of the excitations never closes on this surface. The regions in the parameter space, where there are such nodes on the surface, define the crossover between different quantized plateaus. Thus Eq. **4** allows one to experimentally or numerically map the manifold of degeneracies in the ground state wave function. We will illustrate this point below using an example of an anisotropic spin chain. If in addition the surface can be represented as an invariant closed manifold (such that $\mathcal{F}_{\mu\lambda}$ is constant on this manifold) then Eq. **4** gives a generalization of the integer quantum Hall effect to the abstract parameter space with $\mathcal{F}_{\mu\lambda}$ being a product of a factor of 2π and an integer divided by the surface area. This setup becomes analogous to the Thouless pump (10, 11) with the difference that the quench parameter and the observable are arbitrary and not necessarily related to the particle transport.

Examples

To illustrate how this idea works we will use several specific examples gradually increasing their complexity. First let us consider a spin one-half particle in the external magnetic field described by the Hamiltonian:

$$\mathcal{H} = -\vec{h} \cdot \vec{\sigma}, \qquad \textbf{[7]}$$

where $\vec{\sigma}$ stands for Pauli matrices. It is well known (15) that if we choose a path where h_z is constant, $h_x = h_\perp \cos\phi$, $h_y = h_\perp \sin\phi$ and the angle ϕ changes by 2π (see Fig. 1) then the ground state of the spin acquires the Berry phase:

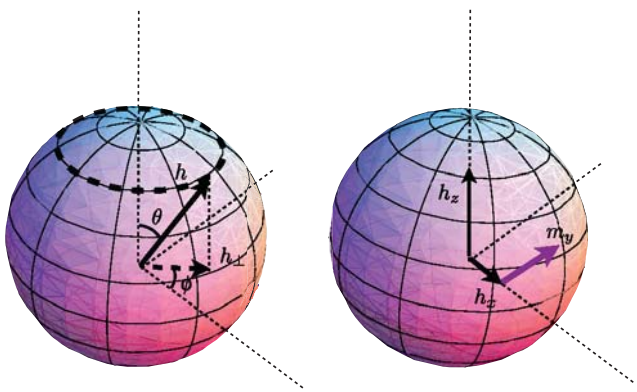

Fig. 1. Two ways of measuring the Berry phase for a spin in a magnetic field: (*i*) Traditional (*Left*) where an external parameter adiabatically changes along a closed path; e.g., by varying the angle ϕ. Then the Berry phase can be measured through the interference signal between the original and the adiabatically evolved spins. (*ii*) Dynamical (*Right*). In this setup one changes an external parameter h_x linearly in time with some velocity v_x and measures the response of the magnetization $m_y(v_x)$. The linear slope of the latter gives the Berry curvature $\mathcal{F}_{yx}$ (see Eq. **4**).

http://doc.rero.ch

$$\gamma = \pi(1 - \cos(\theta)) = \pi\left(1 - \frac{h_z}{h}\right) \qquad \textbf{[8]}$$

A conventional way of measuring the Berry phase in this setup will involve adiabatic motion of the spin around this path and looking into a signal sensitive to the interference of the rotated and the original spins.

Using Eq. **4**, one can obtain the same result in a nonequilibrium protocol which does not directly involve any interference. We will illustrate this with a specific setup. First we prepare the system in the ground state of a magnetic field having a large negative x-component and fixed z-component at the moment $t = t_0$. Then we evolve the magnetic field along the x-direction linearly in time: $h_x(t) = h_x + v_x t$. At time $t = 0$ we measure the magnetization along the y-direction: $m_y = \langle\psi(0)|\sigma_y|\psi(0)\rangle$. This problem is simple enough so that it can be solved analytically using the Weber functions (16), but the solution is quite involved so we solve the Schrödinger equation numerically instead. The result of these simulations for $h_x(t_0) = -99.5$, $h_x = h_x(t = 0) = 0.5$ and $h_z = 1$ is shown in Fig. 2 (solid line). The Berry curvature for this system can be easily computed using an explicit form of the ground state wave function and Eq. **3**. In particular, for $h_y = 0$ it reads:

$$\mathcal{F}_{yx} = \frac{h_z}{2h^3} = \frac{h_z}{2(h_x^2 + h_z^2)^{3/2}} \qquad \textbf{[9]}$$

The linear function $\mathcal{F}_{yx}v_x$ (dashed line) is in perfect agreement with the low velocity asymptotic of the exact solution. From this Berry curvature we can immediately infer the Berry phase along the circular path by noting the rotational invariance of the system:

$$\gamma = \int_0^{2\pi} d\phi \int_0^{h_\perp} d\eta\, \eta \frac{h_z}{2(h_z^2 + \eta^2)^{3/2}} = \pi\left(1 - \frac{h_z}{h}\right), \qquad \textbf{[10]}$$

which is of course the correct result. If the rotational symmetry is broken, one would need to evaluate $\mathcal{F}_{yx}$ in a sufficiently dense set of parameters h_x and h_y enclosed by the closed path and evaluate the area integral over the Berry curvature using finite differences.

To get the first Chern number in this example we can use h_ϕ and h_θ as the external parameters keeping the total magnetic field fixed. Then a similar quench procedure will result in $m_\phi \approx \mathcal{F}_{\phi\theta} v_\theta$, where $\mathcal{F}_{\phi\theta} = 1/2 \sin(\theta)$, which after integration over the spherical surface will result in

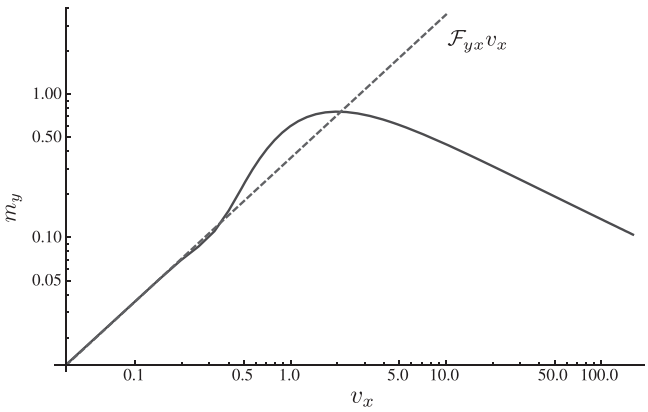

Fig. 2. Magnetization along the y-axis as a function of the quench velocity of the x-component of the magnetic field evaluated at $h_x = 0.5$, $h_y = 0$ and $h_z = 1$. The dashed line is the linear response prediction given by Eq. **4**.

$$ch_1 = \frac{1}{2\pi}\int_0^{2\pi} d\phi \int_0^{\pi} d\theta \frac{1}{2}\sin(\theta) = 1. \qquad \textbf{[11]}$$

The quantization unit here is the system's spin $s = 1/2$.

Next we extend the example above to a Heisenberg spin chain in a magnetic field:

$$\mathcal{H} = -\sum_{j=1}^{N} \vec{h}\,\vec{\sigma}_j - J\sum_{j=1}^{N-1} \vec{\sigma}_j\vec{\sigma}_{j+1}, \qquad \textbf{[12]}$$

where N is the chain size. In this setup we will analyze the response to rotating magnetic field in the θ direction (see Fig. 1) fixing the magnitude $h = 1$:

$$h_x(t) = \sin\left(\frac{v^2t^2}{2\pi}\right), \qquad h_z(t) = \cos\left(\frac{v^2t^2}{2\pi}\right), \qquad h_y(t) = 0. \qquad \textbf{[13]}$$

This choice of time dependence guarantees that the angular velocity is turned on smoothly and the system is not excited at the initial moment of evolution. At the point of measurement $t = \pi/v$ the velocity of the θ-component of the magnetic field is exactly v. As in the previous example we numerically solve the time-dependent Schrödinger equation and evaluate the magnetization along the y axis: $m_\phi = \sum_j \langle\sigma_j^y\rangle$ as a function of the velocity. The slope $\mathcal{F}_{\phi\theta}$ must give the Berry curvature, which we compute as a function of the interaction coupling J.

In order to check the quantization of the first Chern number in this system, one needs to integrate the extracted value of $\mathcal{F}_{\phi\theta}$ over the sphere $h = 1$. However, in this case it is not necessary because of the rotational invariance of the interaction. Thus the integration will result in just the multiplication of $\mathcal{F}_{\phi\theta}$ by the area of the sphere, which is 4π. We thus anticipate that $\mathcal{F}_{\phi\theta}$ is quantized in units of $1/2$ irrespective of the interaction coupling. This is indeed what we observe (Fig. 3). In the ferromagnetic regime ($J \geq 0$) the Berry curvature is equal to $N/2$, which indicates that the ground state behaves as a collective spin of magnitude $S = N/2$. In the antiferromagnetic regime J is large and negative such that the system behaves as a spin singlet $S = 0$ for even N and as an effective spin $1/2$ for odd N. The transition between the spin singlet (for even chain) and the maximally polarized state

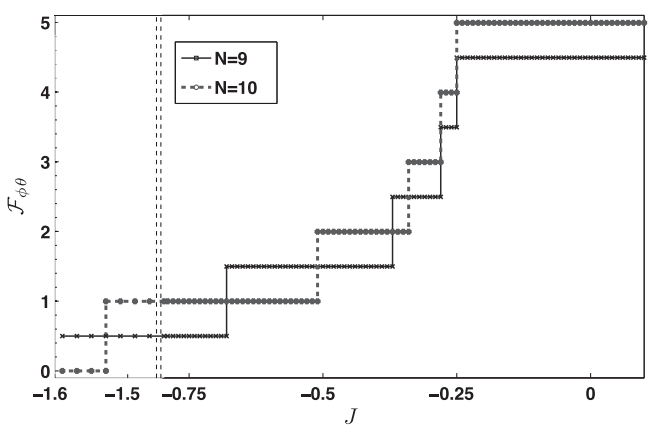

Fig. 3. The Berry curvature extracted from numerically evaluating dynamical response of the magnetization of a Heisenberg spin chain to the rotating magnetic field. The two lines represent chains of the length $N = 9$ and $N = 10$. The quantization plateaus clearly indicate the topological character of the response. Numerical simulations were done by solving the time-dependent Schrödinger equation with fixed velocity $v = 0.1$ (see Eqs. **13** and **13**). The Berry curvature was extracted from the transverse magnetization: $\mathcal{F}_{\phi\theta} \approx m_y(v)/v$.

http://doc.rero.ch

occurs through the quantized steps, which reflect the total value of the spin in the initial state. It is interesting to note that even though we numerically extracted the slope of magnetization $\mathcal{F}_{\phi\theta} \approx M_y(v)/v$ from a moderately small velocity $v = 0.1$, the accuracy of the quantization of plateaus is better than 0.1%.

The example above has still one significant simplification coming from the fact that the magnetization commutes with the Heisenberg interaction term. Therefore, the time evolution of the magnetization is decoupled from the latter. To show that the quantization of the dynamical response holds in a more generic setup we will next consider a disordered (and hence nonintegrable) Heisenberg chain with the Hamiltonian

$$\mathcal{H} = -\vec{h}\sum_{j=1}^{N}\xi_j\vec{\sigma}_j - J\sum_{j=1}^{N-1}\eta_j\vec{\sigma}_j\vec{\sigma}_{j+1}, \qquad \textbf{[14]}$$

where ξ_j and η_j are random variables, which for concreteness are both chosen from a box distribution in the interval [0.75,1.25]. We repeat the same protocol as before—i.e., change the magnetic field according to Eq. **13**—and extract the Berry curvature from the response of the magnetization to the velocity v. In Fig. 4 we show the results of such simulations for a chain of length $N = 9$ with a given realization of disorder. The slopes are extracted from two different velocities $v = 0.1$ and $v = 0.025$. The plot clearly shows that the quantization of the response persists. At higher velocity the crossovers between the plateaus are slightly more rounded and one observes small fluctuations of the numerically extracted $\mathcal{F}_{\phi\theta}$ in the plateau regions. At smaller velocity—i.e., closer to the linear response regime—these fluctuations are suppressed and we see again nearly perfect quantization.

As a final example we analyze an anisotropic chain:

$$\mathcal{H} = -\vec{h}\sum_{j=1}^{N}\vec{\sigma}_j - J\sum_{j=1}^{N-1}(\vec{\sigma}_j^{\perp}\vec{\sigma}_{j+1}^{\perp} + 0.75\sigma_j^z\sigma_{j+1}^z), \qquad \textbf{[15]}$$

where $\vec{\sigma}_j^{\perp}$ denotes x, y components of the spins. This chain has only azimuthal symmetry in the xy plane. In order to get the quantization of the response we thus need to average the Berry curvature over the polar angle of the magnetic field with respect to the z-axis. If we are taking a weak continuous measurement then this average is equivalent to the time average. The results of the numerical simulations for even and odd chains with lengths $N = 9, 10$ are plotted in Fig. 5. To obtain these results we used the

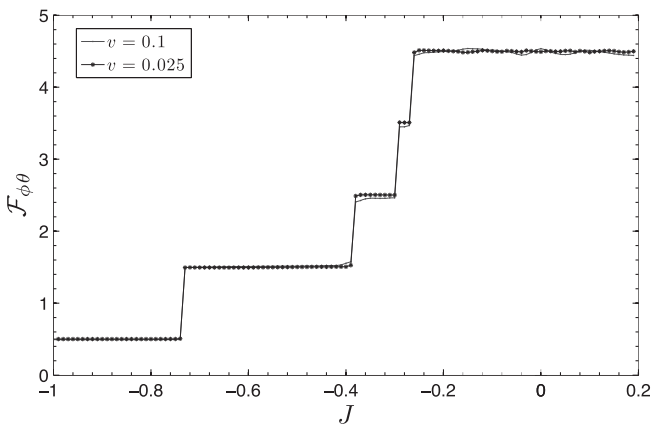

Fig. 4. Berry curvature extracted from dynamical simulations of the disordered Heisenberg chain (see Eq. **14**). The simulations are done for the spin chain of length $N = 9$ using the protocol identical to that in Fig. 3 for a particular realization of the disorder. The two lines represent two different velocities $v = 0.1$ and $v = 0.025$. Smaller velocity clearly improves the accuracy of quantization.

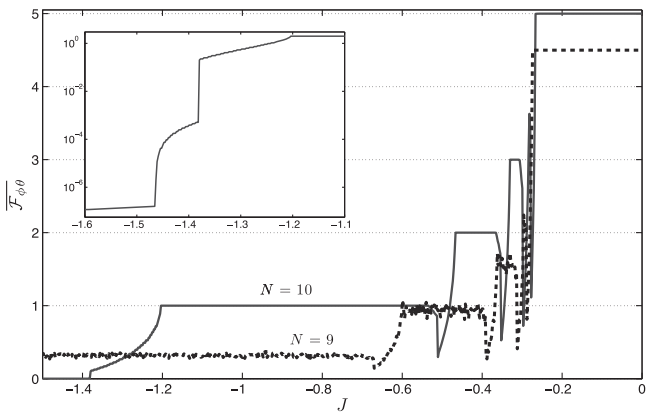

Fig. 5. Berry curvature averaged over the polar angle for the anisotropic spin chain (see Eq. **15**). The simulations are done for spin chains of lengths $N = 9$ and $N = 10$ and the angular velocity $v = 0.025$. The *Inset* shows the result for the even chain in the log scale. Both even and odd chain show a clearly quantized plateau at $J \gtrsim -0.25$ at the value $N/2$. The even chain also shows well-defined plateaus at other integer values. The regions between the plateaus correspond to the regions where the degeneracies of the ground state cross the surface $h =$ const.

same protocol of changing the magnetic field as in Eq. **13** except that we performed an additional averaging over the polar angle. Both chains show clear quantization of the response with $\overline{\mathcal{F}}_{\phi\theta} = N/2$ for $J \gtrsim -0.25$. But at smaller values of J the behavior of the response is different. For odd chain the plateaus have very large fluctuations, while for the even chain the plateaus are perfectly defined. We can understand the odd chain result at large negative J as coming from the double degeneracy of the ground state where the unpaired spin can be localized on the left or right edges of the chain (or alternatively degeneracy between symmetric and antisymmetric combinations of these spins). In a rotationally invariant system these states are protected by the symmetry and there are no transitions between them, so the system behaves as effectively gapped. In an anisotropic chain this protection is lost and thus the ground state is not protected, hence we see no accurate quantization of the plateaus. For the even chain the intervals between the plateaus correspond to the regions where the ground state degeneracies cross the integration surface of constant magnetic field $h = 1$. By deforming the shape of the integration surface such that the jumps between the plateaus become sharp, one can map the precise location of the degeneracies. Analysis of the microscopic origin of this response as well as understanding which plateaus (except for the trivial ones with $\overline{\mathcal{F}}_{\phi\theta}/N = 0, 1/2$) survive in the thermodynamic limit is beyond the scope of this work.

In the examples above we focused on magnetic systems. But our analysis goes through if we consider dipoles in a time-dependent electric field or other setups. For isotropic systems the quantized Berry curvature reveals the total spin of the system. On a more fundamental level this quantization reveals the number of nonequivalent submanifolds of degeneracies of the ground state within the integration surface. In the analyzed examples, for illustration purposes we assumed that the g-factor—i.e. the coupling of spin to the magnetic field—is unity. In real experiments this quantization of the response can be used for a precision measurement of the g-factor like the ordinary quantum Hall effect is used for the precision measurement of e^2/h. Quantization of the integrated Berry curvature can also be used for canceling effects of random static magnetic fields, which might affect accuracy of direct measurements of the magnetization. These and other potential applications will be a subject of future investigation.

http://doc.rero.ch

http://doc.rero.ch

Discussion and Conclusions

Our approach allows an interesting possibility of mapping the Hilbert space topology through quantum dynamics. By measuring the Berry curvature, one can experimentally analyze topological properties of the ground states, extract information about their possible degeneracies, and analyze phase transitions between different topological states. One can also use Berry curvature as a probe of time-reversal symmetry breaking in complicated systems; e.g., in biology.

In conclusion, we demonstrated that the Berry curvature can be measured in generic systems, interacting or not, as a leading nonadiabatic response of physical observables to quench velocity. This method does not require stringent adiabatic conditions hard to achieve in large systems. While in this paper we focused on the quantum dynamics close to the ground state, our main result Eq. **4** applies to the mixed states as well. We illustrated applicability of this method by numerically solving the time-dependent Schrödinger equation for a single spin and different interacting spin chains. In all the cases we found quantization of the dynamical response in agreement with theoretical expectations. This quantization can be interpreted as a dynamical quantum Hall effect. Our findings also reveal deep connections between quantum dynamics and equilibrium geometric properties associated with the adiabatically connected wave functions. We believe that these findings can be used in a variety of systems to experimentally analyze the valuable geometrical properties of the interacting systems without the need to perform sensitive and not always feasible interference experiments.

Methods

Sketch of the Derivation of Eq. 4. Derivation of Eq. **4** is rather simple. It relies on the adiabatic perturbation theory; i.e., perturbation theory in the instantaneous basis (17, 18). For linear quenches one finds that the transition amplitude to the nth eigenstate of the final Hamiltonian is (18)

$$a_n \approx i v_\lambda \frac{\langle n|\partial_\lambda|0\rangle}{(\varepsilon_n-\varepsilon_0)} e^{-i\Theta_{n0}}\Big|_{\lambda_i}^{\lambda_f} = -i v_\lambda \frac{\langle n|\partial_\lambda \mathscr{H}|0\rangle}{(\varepsilon_n-\varepsilon_0)^2} e^{-i\Theta_{n0}}\Big|_{\lambda_i}^{\lambda_f}, \qquad [16]$$

where Θ_{n0} is the full phase difference (including the dynamical and the Berry phases) between the nth and the ground instantaneous eigenstates during time evolution:

$$\Theta_{n0}(\lambda) = \int_\lambda^{\lambda_f} d\lambda' \left[\frac{\varepsilon_n(\lambda')-\varepsilon_0(\lambda')}{v(\lambda')} - i(\mathscr{A}_n(\lambda')-\mathscr{A}_0(\lambda'))\right]. \qquad [17]$$

If the initial state has a large gap or if the protocol is designed in such a way that the initial evolution is adiabatic, then Eq. **16** takes a particularly simple form:

$$a_n \approx -i v_\lambda \frac{\langle n|\partial_\lambda \mathscr{H}|0\rangle}{(\varepsilon_n-\varepsilon_0)^2}\Big|_{\lambda_f} \qquad [18]$$

The contribution of the initial term in Eq. **16** to the expectation value of the off-diagonal observables can be additionally suppressed by the fast oscillating phase Θ_{n0}. This suppression will happen even if by magnitude this contribution is comparable to the final term (**18**). Let us note that in order to obtain this result from Eq. **19**, in Ref. (18) one needs to perform an additional phase transformation to undo the transformations given by Eqs. **6** and (**14**) of that work. Let us also point that Eq. **18** is equivalent to Eq. 2.10 in Ref. (11) for a particular choice of parameters. However, as we discuss above, this result is only valid provided that the initial term in a more general Eq. **16** is unimportant.

From Eq. **18** it is straightforward to derive Eq. **4**:

$$\mathscr{M}_\mu = \langle\psi| - \partial_\mu \mathscr{H}|\psi\rangle \approx \langle 0| - \partial_\mu \mathscr{H}|0\rangle + i v_\lambda \sum_{n\neq 0} \frac{\langle 0|\partial_\mu \mathscr{H}|n\rangle\langle n|\partial_\lambda \mathscr{H}|0\rangle - \mu\leftrightarrow\lambda}{(\varepsilon_n-\varepsilon_0)^2} \qquad [19]$$

It is easy to check that the second term in this equation is equivalent to Eq. **4**.

Application of Eq. 4 to the Integer Quantum Hall Effect. He we elaborate on that the quantum Hall effect can be understood as a particular application of Eq. **4**. This discussion will closely follow the first chapter of Ref. (19).

The Hall current in the ordinary setup can be derived using the adiabatic transport theory combined with the Kubo formula. To compute the Hall conductivity one usually applies the adiabatic formulas similar to those derived in Appendix A, to some in general interacting Hamiltonian $\mathscr{H}(A_x(t), A_y(t))$ on a torus of size $L_x \times L_y$. The Hamiltonian $\mathscr{H}$ depends on the vector potential of the fixed external magnetic field A^{mag} and on slowly varying perturbations θ and ϕ,

$$A_x(t) = A_x^{\text{mag}} + \phi/L_x, \qquad [20]$$

$$A_y(t) = A_y^{\text{mag}} + \theta/L_y, \qquad [21]$$

The current operators I_x and I_y are given by

$$I_x = \frac{\partial \mathscr{H}}{\partial \phi}, \qquad I_y = \frac{\partial \mathscr{H}}{\partial \theta}. \qquad [22]$$

One imposes the external Hall voltage ε by varying the parameter θ in time. In particular, from $\partial_t A_y = E_y$ and $-L_y E_y = \varepsilon$ we see that $\partial_t \theta = \varepsilon$. Thus we can view the Hall voltage as the rate of change of the parameter θ. Explicitly applying the expressions for the transition amplitudes derived in the previous appendix, we get that in the linear response

$$\langle I_x\rangle = i \sum_{m\neq 0} \frac{\langle 0|I_x|m\rangle\langle m|I_y|0\rangle - x\leftrightarrow y}{(\varepsilon_m-\varepsilon_0)^2}\dot{\theta}. \qquad [23]$$

where $|0\rangle$ is an instantaneous ground state. The first term in the right-hand side of this equation is exactly the curvature of the Berry phase in the space of parameters θ and ϕ:

$$\mathscr{F}_{\theta\phi} = i\left(\langle 0|\overleftarrow{\partial}_\theta \partial_\phi|0\rangle - \langle 0|\overleftarrow{\partial}_\phi \partial_\theta|0\rangle\right) \qquad [24]$$

Averaging the Berry curvature over θ, ϕ is equivalent to the evaluation of the (first) Chern character:

$$ch_1(|0\rangle) = \frac{1}{2\pi}\int_{T^2} d\theta d\phi \mathscr{F}_{\theta\phi}, \qquad [25]$$

which is an integer number. This result gives the well-known topological quantization condition of the Hall conductivity:

$$\sigma_H = \frac{e^2}{2\pi h} ch_1(|0\rangle) \qquad [26]$$

Note added. After this work was complete we became aware of a recent paper (20), where partially overlapping results were obtained.

ACKNOWLEDGMENTS. We acknowledge useful discussions with C. Chamon, C. De Grandi, P. Hanggi, G. Ortiz, A. Sandvik, and M. Tomka. The work was supported by Grants National Science Foundation DMR-0907039 (A.P.), Air Force Office of Scientific Research FA9550-10-1-0110 (A.P.), the Sloan Foundation (A.P.), and by Swiss National Science Foundation (V.G.).

1. Berry M (1984) Quantal phase factors accompanying adiabatic changes. *Proc R Soc Lond Ser A* 392:45–47.
2. Griffiths DJ (2005) *Introduction to Quantum Mechanics* (Pearson, Upper Saddle River, NJ), Second Edition.
3. Provost JP, Vallee G (1980) Riemannian structure on manifolds of quantum states. *Comm Math Phys* 76:289–301.
4. Venuti LC, Zanardi P (2007) Quantum critical scaling of geometric tensors. *Phys Rev Lett* 99:095701.
5. Zhang YB, Tan YW, Stormer HL, Kim P (2005) Experimental observation of the quantum Hall effect and Berry's phase in graphene. *Nature* 438:201.
6. Tomita Akira, Chiao Raymond Y (1986) Observation of Berry's topological phase by use of an optical fiber. *Phys Rev Lett* 57:937–940.
7. Haldane FDM (1987) Comment on "Observation of Berry's topological phase by use of an optical fiber". *Phys Rev Lett* 59:1788–1788.
8. Haldane FDM (2004) Berry curvature on the fermi surface: Anomalous hall effect as a topological fermi-liquid property. *Phys Rev Lett* 93:206602.
9. Ortiz G (2001) *The geometry of quantum phase transitions, chapter in* Understanding Quantum Phase Transitions, ed L Carr (CRC Press, New York).
10. Thouless DJ (1983) Quantization of particle transport. *Phys Rev B* 27:6083–6087.
11. Niu Q, Thouless DJ (1984) Quantised adiabatic charge transport in the presence of substrate disorder and many-body interaction. *J Phys A: Math Gen* 17:2453–2462.
12. Xiao D, Chang M-C, Niu Q (2010) Berry phase effects on electronic properties. *Rev Mod Phys* 82:1959–2007.
13. De Grandi C, Polkovnikov A, Sandvik AW (2011) Universal nonequilibrium quantum dynamics in imaginary time. *Phys Rev B* 84:224303.
14. Berry MV, Robbins JM (1993) Chaotic classical and half classical adiabatic reactions: Geometric magnetism and deterministic friction. *Proc R Soc London* 442:659–672.
15. Sakurai JJ (2005) *Modern Quantum Mechanics, Revised Edition* (Addison-Wesley, Reading, MA).
16. Vitanov NV (1999) Transition times in the landau-zener model. *Phys Rev A* 59:988.
17. Rigolin G, Ortiz G, Ponce VH (2008) Beyond the quantum adiabatic approximation: Adiabatic perturbation theory. *Phys Rev A* 78:052508.
18. De Grandi C, Polkovnikov A (2010) Adiabatic perturbation theory: From landau-zener problem to quenching through a quantum critical point. *Lect Notes Phys* 802:75–114.
19. Stone M, ed. (1992) *Quantum Hall Effect* (World Scientific, Teaneck, NJ).
20. Avron JE, Fraas M, Graf GM, Kenneth O (2011) Quantum response of dephasing open systems. *New J Phys* 13:053042.

http://doc.rero.ch